2007

PECVD grown DBR for microcavity OLED sensor

Brandon Scott Bohlen
Iowa State University

PECVD grown DBR for microcavity OLED sensor

by

Brandon Scott Bohlen

A thesis submitted to the graduate faculty

in partial fulfillment of the requirements for the degree of

MASTER OF SCIENCE

Major: Electrical Engineering

Program of Study Committee:
Gary Tuttle, Major Professor
Santosh Pandey
L. Scott Chumbley

Iowa State University

Ames, Iowa

2007

TABLE OF CONTENTS

LIST OF TABLES

LIST OF FIGURES

ACKNOWLEDGEMENTS

I would like to thank the following people for their support during the completion of this work. Dr. Tuttle for being my major professor and an excellent teacher and "boss". Max Noack and Daniel Stieler for their intellectual and technical support and comradery. Abby Kime and my parents, Scott and Jacqueline Bohlen, for their support and motivation. Jane Woline and Pam Myers for their administrative help and support. Santosh Pandey and Scott Chumbley for being excellent teachers and for serving on my POS committee.

"Thank You." - Brandon

ABSTRACT

Organic light emitting devices (OLED) have become a popular topic of research and product development in the past decade. The use of OLEDs as the light source in a compact photoluminescent sensor has been studied for the detection of various chemicals. Controlling the bandwidth of light emitted by the OLED would be beneficial to the sensitivity of these sensors. By building the OLEDs in a microcavity structure, the bandwidth and peak frequency of light being emitted can be controlled and adjusted to a specific value.

A key component of a microcavity is a partially transmitting reflector: a reflector with less than 90% reflectance. A dielectric mirror can be manufactured with varying reflectance and can be well integrated into the OLED manufacturing process. The dielectric mirror created for this project is a distributed Bragg reflector (DBR) made of alternating silicon nitride and silicon dioxide layers. The layers were grown with plasma-enhanced chemical vapor deposition (PECVD); a low temperature, low pressure deposition system. Building a DBR using PECVD allows for the creation of the reflector on any surface that can withstand temperatures of approximately 300°C and takes less than an hour to make up to four mirrors.

The growth rate of silicon nitride and silicon dioxide films from plasma enhanced chemical vapor deposition of silane, ammonia, and nitrous oxide was characterized. The PECVD system has no growth rate measurement capabilities, therefore characterization was the only way to determine the ultimate growth parameters for this project.

A repeatable method for the manufacture of silicon dioxide/nitride distributed Bragg reflectors for use in microcavity OLED sensors was designed. Three DBRs were grown on glass slides and measured with a spectrophotometer. The three slides had reflectance of between 75% and 85% with full widths at half maximum of 170-180nm centered around 570-590nm.

CHAPTER 1. INTRODUCTION

Optical microcavities have been utilized in electronics for many purposes. These purposes include: to induce lasing, to increase efficiency of light emitting diodes, to increase the speed of communications, and even to implement quantum computing. Joseph Shinar's research group has been using organic light emitting diodes (OLEDs) as the light source in photoluminescence-based sensors (4). By adding a microcavity structure to the OLEDs in these sensors, the wavelength of the light can be controlled and the bandwidth narrowed, thus, allowing for the design of more selective sensors.

The goal of this project was to create a repeatable method for making distributed Bragg reflectors (DBRs) as a base for the completion of OLED microcavities. The construction method used was plasma-enhanced chemical vapor deposition (PECVD) of silicon dioxide and silicon nitride.

Plasma-enhanced chemical vapor deposition (PECVD) is a thin film deposition system in common use in the semiconductor industry. PECVD allows for the deposition of insulators without the use of high temperatures. Because of this, PECVD can be used to deposit films directly on top of metals, such as the aluminum cathode of an OLED. The use of PECVD for the creation of the DBR allows for easy integration of the manufacturing process into the production of OLEDs.

A distributed Bragg reflector is a dielectric mirror. By stacking alternating layers of high and low dielectric materials, with the correct thicknesses, light of a specific wavelength is reflected through constructive interference. A DBR can then be used as a semi-transparent mirror for one side of an optical microcavity, allowing the light to escape.

Organic light emitting diodes conduct electricity through an electroluminescent organic

compound, causing it to emit light. By combining an OLED with a photoluminescent (PL) material, researchers have been able to create a compact glucose sensor (4). A microcavity structure can narrow the frequency of light produced by the OLED, allowing the PL sensor can be tuned to detect specific materials such as glucose, oxygen, alcohol, or anthrax. The addition of a microcavity structure to these OLEDs will allow the production of light sources that produce a narrower bandwidth of light and possibly devices with higher efficiencies (5).

CHAPTER 2. BACKGROUND

2.1 PECVD

2.1.1 Operation

The plasma-enhanced chemical vapor deposition system used in this project creates a plasma through capacitive-coupling of radio frequency (RF) power. The system uses a 13.56MHz amplifier to supply power to the top plate of a pair of plates in a vacuum chamber. Gas is sent into the chamber and flows out from the bottom plate (platen), placing all the reactant gases between the plates, in the "dielectric" region of the capacitor. Energy from the RF field between plates is transferred into the reactant gases, causing them to dissociate into ionized precursors of the desired deposition materials. Substrates are placed on the heated platen. The heated substrate acts as a catalytic surface for the precursor gases (in plasma form) to assemble into new molecules.

The three reactant gases used in this project are silane (SiH_4), ammonia (NH_3), and nitrous oxide (N_2O). Silane and ammonia are used to produce silicon nitride (Si_3N_4) and silane and nitrous oxide are used to produce silicon dioxide (SiO_2). The creation of precursors to silicon nitride by the ammonia and silane plasma interaction is shown in Equation 2.1 (10). The surface reaction is shown in Equation 2.2 (10).

$$SiH_4 + 4NH_3 \overset{plasma}{\longrightarrow} Si\left(NH_2\right)_4 + 4H_2 \tag{2.1}$$

$$3Si\left(NH_2\right)_4 \overset{heat}{\longrightarrow} Si_3N_4 + 8NH_3 \uparrow \tag{2.2}$$

The reaction of silane and nitrous oxide to form silicon dioxide is shown in Equation 2.3 (8). The reaction of silane and nitrous oxide is known to create a precursor, $Si(OH)_4$, similar to the creation of $Si(NH_2)_4$ from the silane/ammonia reaction. However, this precursor is unlikely to be the precursor to silicon dioxide as it would create a film with compressive stress, while the silicon dioxide film created in the PECVD process is composed of molecules under tensile stress (10).

$$SiH_4 + 2N_2O \overset{plasma}{\longrightarrow} SiO_2 \downarrow +2N_2 \uparrow +2H_2 \uparrow \tag{2.3}$$

2.1.2 Applications

PECVD systems are used throughout the semiconductor industry. PECVD is used to apply the passivation layer to the top of the semiconductor after metal deposition to electrically insulate the various devices and metal layers from one another. Deposition on metal is possible because of the relatively low temperatures required for deposition compared to other CVD techniques. Modern PECVD systems have been developed to allow for faster throughput and can deposit materials with even thickness across 300mm diameter wafers with excellent precision.

2.2 DBR

2.2.1 Physics

A distributed Bragg reflector works on the principle of light wave interference. Utilizing the refractive properties of transparent materials, a DBR can create a mirror with near perfect reflectivity. As shown in Figure 2.1, light enters the DBR from the left and, as it encounters an interface between two materials with different refractive indices, the light is both transmitted and reflected. If the optical thicknesses of these materials is one-fourth the wavelength of light traveling through the reflector, the phases of these reflected waves are aligned to create constructive interference (6).

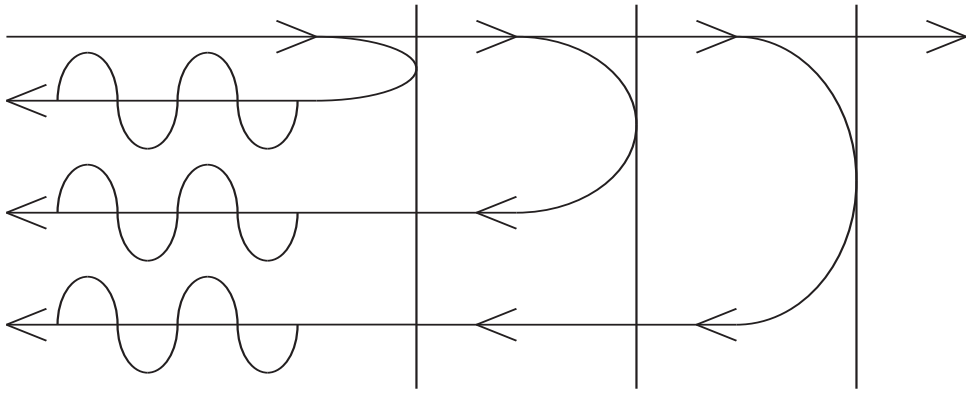

Figure 2.1 A schematic depiction of the reflections in a DBR

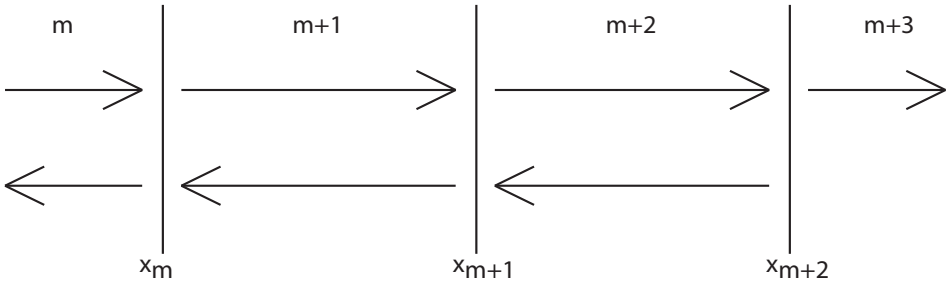

Figure 2.2 A DBR showing the direction of propagation of E-M waves

The interactions between interfaces can be accurately described in terms of electromagnetic (E-M) waves propagating through the DBR. Figure 2.2 shows the propagation of E-M waves through two finite thickness layers, $m+1$ and $m+2$ and two infinite thickness environments, m and $m+3$. Using Maxwell's equations and treating each layer as a one-dimensional (thickness) plane, we are able to describe a stack of such layers in terms of a matrix. Starting in layer m, the E-M wave has electric and magnetic field properties of the form shown in Equations 2.4 and 2.5, respectively.

$$E_m(x) = E_m^+ \exp\left[ik_m\left(x - x_m\right)\right] + E_m^- \exp\left[-ik_m\left(x - x_m\right)\right] \tag{2.4}$$

$$H_m(x) = \frac{E_m^+}{Z_m} \exp\left[ik_m\left(x - x_m\right)\right] - \frac{E_m^-}{Z_m} \exp\left[-ik_m\left(x - x_m\right)\right] \tag{2.5}$$

The waves in the $m+1$ region can be described similarly as shown in Equations 2.6 and 2.7.

$$E_{m+1}(x) = E_{m+1}^+ \exp\left[ik_{m+1}\left(x - x_m\right)\right] + E_{m+1}^- \exp\left[-ik_{m+1}\left(x - x_m\right)\right] \tag{2.6}$$

$$H_{m+1}(x) = \frac{E_{m+1}^+}{Z_{m+1}} \exp\left[ik_{m+1}\left(x - x_m\right)\right] - \frac{E_{m+1}^-}{Z_{m+1}} \exp\left[-ik_{m+1}\left(x - x_m\right)\right] \tag{2.7}$$

The boundary conditions for electromagnetic waves at the interface of two lossless materials requires that both the E and H field waves are continuous (3). Therefore, at x_m Equation 2.4 can be set equal to Equation 2.6 and Equation 2.5 equal to 2.7 as shown in Equations 2.8 and 2.9.

$$E_m(x_m) = E_m^+ + E_m^- = E_{m+1}(x_m) = E_{m+1}^+ + E_{m+1}^- \tag{2.8}$$

$$H_m(x_m) = \frac{E_m^+}{Z_m} - \frac{E_m^-}{Z_m} = H_{m+1}(x_m) = \frac{E_{m+1}^+}{Z_{m+1}} - \frac{E_{m+1}^-}{Z_{m+1}} \tag{2.9}$$

Solving for the fields in layer m in terms of the fields in layer $m+1$ from Equations 2.8 and 2.9 yields Equations 2.10 and 2.11.

$$E_m^+ = \left[\frac{Z_{m+1} + Z_m}{2Z_{m+1}}\right] E_{m+1}^+ + \left[\frac{Z_{m+1} - Z_m}{2Z_{m+1}}\right] E_{m+1}^- \tag{2.10}$$

$$E_m^- = \left[\frac{Z_{m+1} - Z_m}{2Z_{m+1}}\right] E_{m+1}^+ + \left[\frac{Z_{m+1} + Z_m}{2Z_{m+1}}\right] E_{m+1}^- \tag{2.11}$$

Writing these equations in matrix form gives the interface matrix, $I_{m,m+1}$, where $[E_m] = [I_{m,m+1}] \times [E_{m+1}]$ as shown in Equation 2.12.

$$\begin{bmatrix} E_m^+ \\ E_m^- \end{bmatrix} = \begin{bmatrix} \left(\frac{1}{2} + \frac{Z_m}{2Z_{m+1}}\right) & \left(\frac{1}{2} - \frac{Z_m}{2Z_{m+1}}\right) \\ \left(\frac{1}{2} - \frac{Z_m}{2Z_{m+1}}\right) & \left(\frac{1}{2} + \frac{Z_m}{2Z_{m+1}}\right) \end{bmatrix} \begin{bmatrix} E_{m+1}^+ \\ E_{m+1}^- \end{bmatrix} \tag{2.12}$$

When placed in terms of refractive index (n) rather than wave impedance (Z), $I_{m,m+1}$ in Equation 2.12 becomes Equation 2.13.

$$I_{m,m+1} = \begin{bmatrix} \left(\frac{1}{2} + \frac{n_{m+1}}{2n_m}\right) & \left(\frac{1}{2} - \frac{n_{m+1}}{2n_m}\right) \\ \left(\frac{1}{2} - \frac{n_{m+1}}{2n_m}\right) & \left(\frac{1}{2} + \frac{n_{m+1}}{2n_m}\right) \end{bmatrix} \tag{2.13}$$

In addition to their interface reaction, the E-M waves traveling through each layer will undergo some phase change, which can also be described in matrix form. The propagation of waves traveling through layer $m+1$ is described in Equations 2.14 and 2.15. These equations can be combined into a matrix, P_{m+1}, describing the propagation through layer $m+1$ as shown in Equation 2.16, where $L_{m+1} = x_{m+1} - x_m$ is the thickness of layer $m+1$.

$$E_{m+1}^+(x_{m+1}) = E_{m+1}^+(x_m) \exp\left[ik_{m+1}\left(x_{m+1} - x_m\right)\right] \tag{2.14}$$

$$E_{m+1}^-(x_m) = E_{m+1}^-(x_{m+1}) \exp\left[ik_{m+1}\left(x_{m+1} - x_m\right)\right] \tag{2.15}$$

$$\begin{bmatrix} E_m^+\left(x_m\right) \\ E_m^-\left(x_m\right) \end{bmatrix} = \begin{bmatrix} \exp\left[-ik_{m+1}L_{m+1}\right] & 0 \\ 0 & \exp\left[ik_{m+1}L_{m+1}\right] \end{bmatrix} \begin{bmatrix} E_{m+1}^+\left(x_{m+1}\right) \\ E_{m+1}^-\left(x_{m+1}\right) \end{bmatrix} \tag{2.16}$$

Using these interface and propagation matrices, a simple equation can be assembled to describe a complex model containing many layers of materials. With Figure 2.2 as a guide, a matrix equation can be created as shown in Equations 2.17 and 2.18.

$$\begin{bmatrix} E_m^+ \\ E_m^- \end{bmatrix} = I_{m,m+1}P_{m+1}I_{m+1,m+2}P_{m+2}I_{m+2,m+3} \begin{bmatrix} E_{m+3}^+ \\ E_{m+3}^- \end{bmatrix} \tag{2.17}$$

$$I_{m,m+1}P_{m+1}I_{m+1,m+2}P_{m+2}I_{m+2,m+3} = \begin{bmatrix} M_{11} & M_{12} \\ M_{21} & M_{22} \end{bmatrix} \tag{2.18}$$

Assuming light only enters the model from the left side, E^-_{m+3} can be set equal to zero and the reflectance of the model can be described using only the propagation/interface matrix shown in Equation 2.18. The equation for reflectance, R, is shown in Equation 2.19.

$$R = \frac{\frac{|E^-_m|^2}{Z_m}}{\frac{|E^+_m|^2}{Z_m}} = \frac{\left|M_{21}E^-_{m+3}\right|^2}{\left|M_{11}E^+_{m+3}\right|^2} = \left|\frac{M_{21}}{M_{11}}\right|^2 \tag{2.19}$$

Using this matrix method for solving the reflectance of a multilayer stack, a computer program was created to model the reflectance spectrum of DBRs. Using a model of 5 pairs of reflecting layers on a substrate of glass and an atmosphere of air, a reflectance spectrum was created. The model was based on alternating layers of silicon dioxide and silicon nitride. Silicon dioxide has a refractive index of 1.45 and silicon nitride has a refractive index of 2.0. From these indices the thickness of each layer was calculated for a base frequency of 538nm as shown in Equation 2.20.

$$\lambda = \frac{\lambda_0}{n}; \lambda_{SiO_2} = \frac{\frac{538nm}{4}}{1.45} = 92.76nm; \lambda_{Si_3N_4} = \frac{\frac{538nm}{4}}{2.0} = 67.25nm \tag{2.20}$$

These layers were stacked (nitride, oxide, nitride, etc) on top of a glass substrate, creating the reflector shown in Figure 2.3

The reflectance produced by this model is shown in Figure 2.4. This DBR has reflectance of over 70% across wavelengths of approximately 500 to 600nm and is only 805nm thick.

2.2.2 Applications

Distributed Bragg reflectors have been used for a number of applications in communications, research, and manufacturing. The most common use of DBRs is as one or both of the reflectors in a distributed feedback laser (6). This type of laser places the light emitting device between two mirrors that are separated by a distance equal to a multiple of the wavelength of light being

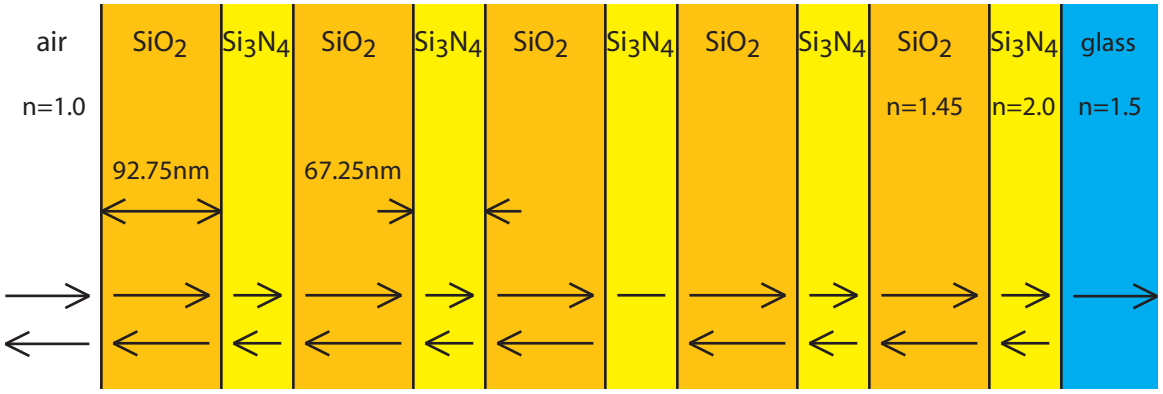

Figure 2.3 A distributed Bragg reflector with 5 pairs of layers

emitted. This configuration amplifies the light through constructive interference. Because of the stopband capabilities and high reflectivity of DBRs, they make excellent reflectors for single-frequency laser diodes. Also, for these lasers to work properly, one of the reflectors must be semi-transmitting and DBRs can be designed with reflectivity ranging from 30-100%. Such lasers have been used for optical communications, laser metrology and have even been modified to design tunable lasers for research. With the increase in use of chemical vapor deposition by the semiconductor industry, DBR mirrors can be manufactured easily and integrated directly into the manufacturing process of a semiconductor laser.

2.2.3 Implementation

A distributed Bragg reflector similar to the one described in Figures 2.3 and 2.4 was built for this project utilizing PECVD techniques. The reflector was grown on glass slides to be used as a base for an OLED microcavity. After completion of the reflector a layer of indium tin oxide can be deposited as the anode of the OLED. Next a layer of organic electroluminescent materials can be deposited followed by an aluminum cathode. This stack of materials will create a microcavity OLED capable of producing a narrow band of light with wavelengths in the 500nm range. This narrow frequency OLED can then be used as the light source in a compact photoluminescent sensor capable of detecting oxygen, glucose, alcohol, or other chemicals.

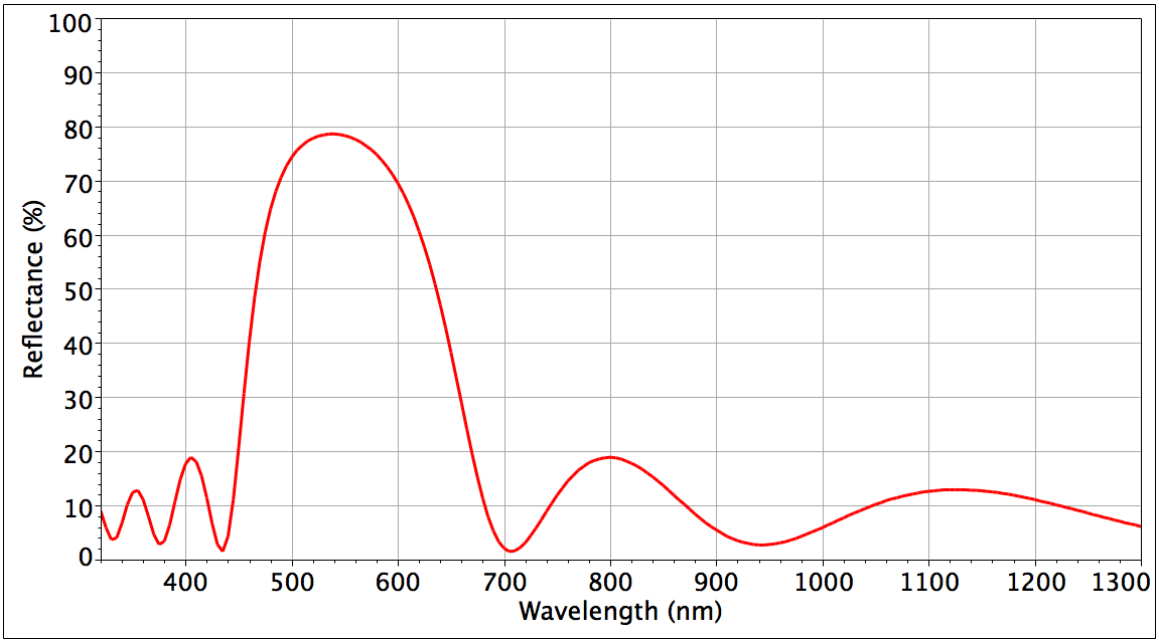

Figure 2.4 Reflectance by wavelength of a DBR with 5 pairs of layers

2.3 OLED

2.3.1 Operational Theory

Organic light emitting diodes work on the principle of electroluminescence. Electroluminescence is the mechanism in which certain organic compounds will emit light when electricity flows through them. OLEDs utilize this mechanism by sandwiching an emissive layer between electron and hole transport layers and electrodes. Figure 2.5 shows the structure and operation of an OLED. The cathode acts as a source for electrons and the anode for holes. As electrons are drawn toward the anode (and holes toward the cathode) through electric field forces, the transport layers act as energy ramps, allowing the electrons and holes to transition smoothly from the cathode into the organic layer. The electrons must pass through the organic material to reach their higher potential destination. Inside the organic layer, holes and electrons meet, recombine, and emit light.

The organic layer can be described in terms of its lowest unoccupied molecular orbital (LUMO) and highest occupied molecular orbital (HOMO) bands. The LUMO and HOMO

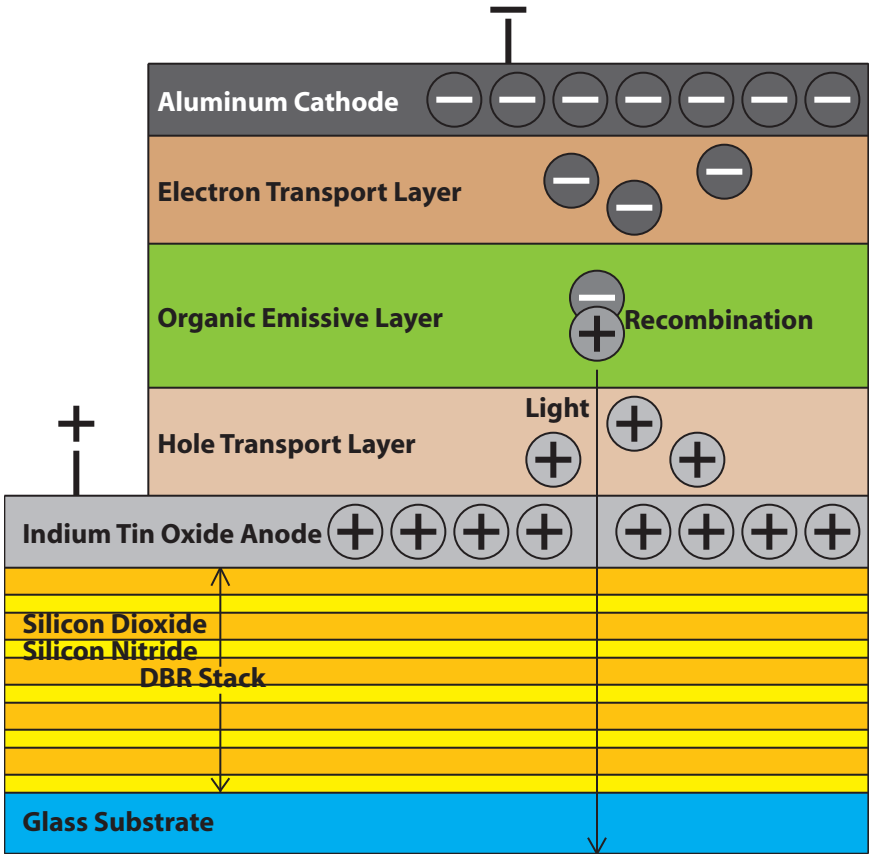

Figure 2.5 OLED microcavity structure and operation

bands are analogous to the conduction and valence bands of a semiconductor, respectively. The purpose of the transport layers is to gradually adjust these band levels from the organic layer to the metal cathode and anode, so the interface between the two is less abrupt and the flow of electrons and holes isn't impeded. By creating a small abrupt transition from the transport layer to the organic layer, an electron trap is created. This trap builds up an abundance of electrons and becomes the point of recombination with holes and thus the point of light emission.

2.3.2 Applications

Due to advanced research into new organic materials in recent years, OLEDs have gained a strong foothold in the electronics market. OLED televisions are months away from reaching the

consumer market in Japan and have also been used to design white lighting that will replace incandescent bulbs with a much greater lumens per watt efficiency. OLEDs are capable of being manufactured on flexible and/or transparent substrates, allowing for innovative product designs. OLED displays have been utilized in cellphones, electric razors, watches and other devices where LCDs have been used in the past. OLED displays are capable of producing high brightness and increased contrast because they utilize active pixels, rather than backlit LCD pixels. Unlike LCDs, OLEDs have little to no temperature sensitivity. OLEDs are 75% more efficient than LCDs, and much thinner. Because OLEDs can be built with transparent electrodes, they can be stacked into pixels used to produce even higher resolution displays than today's modern high definition televisions and computer monitors.

CHAPTER 3. PECVD DEPOSITION

3.1 Equipment

Film growth was performed with a 900 Series Plasma Enhanced Chemical Vapor Deposition System, built by Technics, Inc. of Dublin, CA. The Technics system (shown in Figure 3.1) consists of a parallel plate chamber, three source gas mass-flow controllers, a mechanical vacuum pump, a heated platen with temperature controller, and a 300W, 13.56 MHz RF amplifier.

This system creates a plasma through capacitive induction of RF waves in which the top plate of the chamber acts as the antenna and the bottom plate (platen) is at ground. Gases flow into the chamber through 12 angled holes in the platen creating a symmetrical cloud between the plates, where the substrates rest. An MFJ-969 tuning network was added to match the impedance of the plasma to the amplifier.

Several controls exist that allow the user to adjust the flow rate of gases, the pressure of the system, the power of the RF amplifier output, and the substrate temperature. Additionally, there are switches to turn on or off the flow of gases or the vacuum presence. A valve is located between the mechanical vacuum pump and the chamber that allows the user to adjust the pressure of the system by partially blocking the vacuum flow from the chamber.

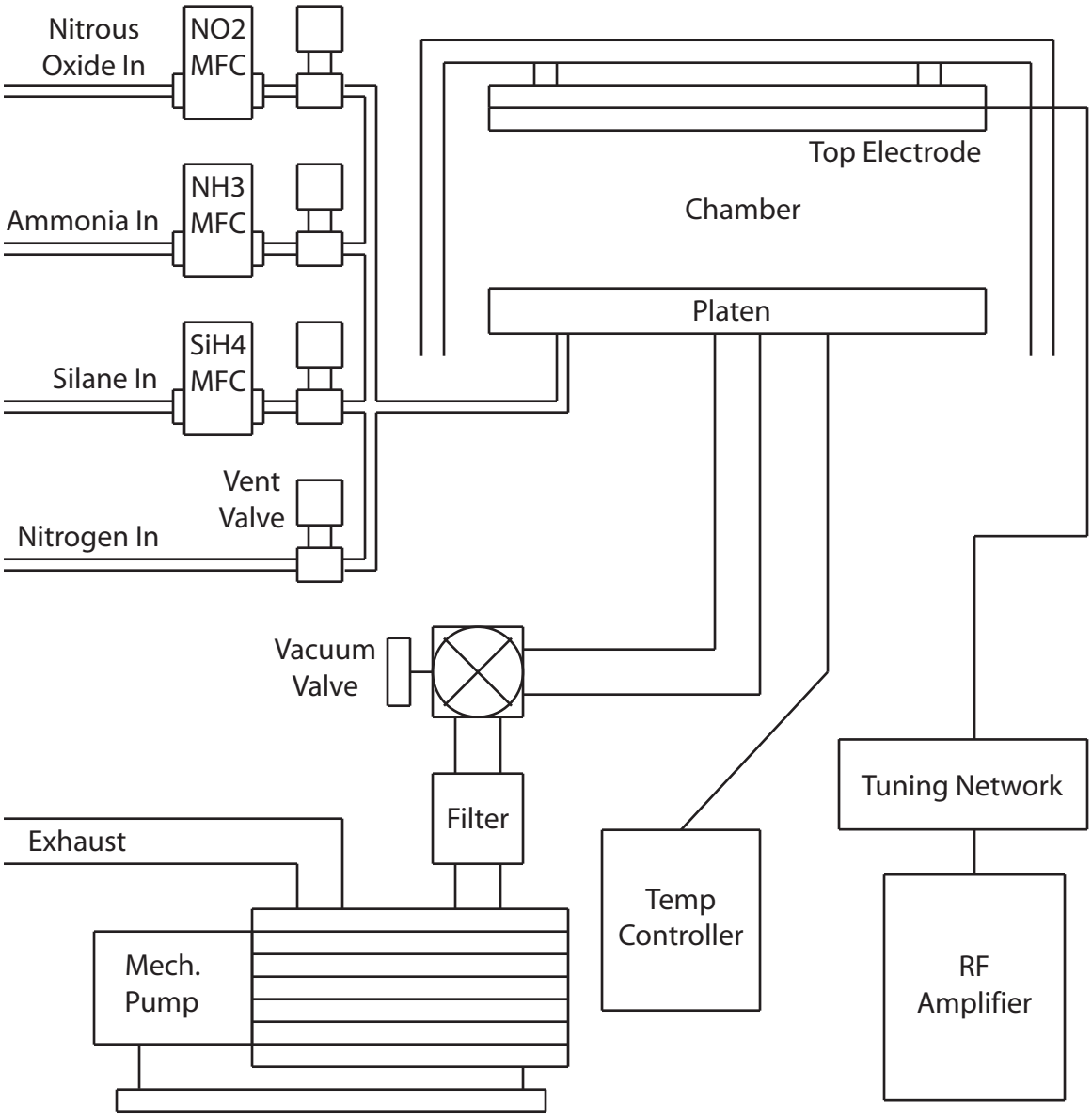

Figure 3.1 PECVD system structure

3.2 Method

3.2.1 Design

The PECVD system used does not contain any growth rate measurement sensors. Experiments were designed to determine the effects of pressure, flow rate, and RF power on growth rate. Experiments were also performed to determine the repeatability of the growth rate at determined parameters based on the previous tests.

The suggested parameters for growth in the Technics manual are shown in Table 3.1(11). The suggested flow rates did produce approximately 500mTorr of pressure in the chamber with the vacuum valve completely open, however, in order to obtain a range of pressures above and below 500mTorr the flow rates were reduced by half for characterization experiments.

Table 3.1 Technics growth parameters

Process	**Gas**	**Flow (sccm)**	**Chamber Pressure**	**Platen Temp**	**Power Level**
Silicon Nitride	SiH_4	20	500mTorr	200–350°C	50–75W
	NH_3	55			
Silicon Dioxide	SiH_4	20	500mTorr	200–350°C	50–75W
	N_2O	60			

Pressure and RF power were determined to be the more important parameters to growth rate and refractive index, based on a literature survey. Little evidence was found on the effects of temperature on PECVD growth and the goal for these growths was to utilize low temperatures, so temperature experiments were not performed. Experiments were designed as shown in Table 3.2 to determine the optimum parameters for growth of silicon dioxide and silicon nitride. Since the final goal for the use of this system was to grow alternating films of silicon dioxide and silicon nitride, the experiments for both films were kept as similar as possible so that the growth of DBRs would be an easy and relatively quick process.

Table 3.2 Experiment growth parameters

Wafer No.	Process	Gas	Flow (sccm)	Platen Temp	Time	Chamber Pressure	Power Level
1	Silicon Dioxide	SiH_4	10	280°C	30min	500mTorr	20W
		N_2O	30				
2	”	”	”	”	”	”	40W
3	”	”	”	”	”	”	60W
4	”	”	”	”	”	”	80W
5	”	”	”	”	”	”	100W
6	Silicon Dioxide	SiH_4	10	280°C	30min	320mTorr	75W
		N_2O	30				
7	”	”	”	”	”	400mTorr	”
8	”	”	”	”	”	500mTorr	”
9	”	”	”	”	”	600mTorr	”
10	”	”	”	”	”	700mTorr	”
16	Silicon Nitride	SiH_4	10	280°C	30min	500mTorr	20W
		NH_3	27.5				
17	”	”	”	”	”	”	40W
18	”	”	”	”	”	”	60W
19	”	”	”	”	”	”	80W
20	”	”	”	”	”	”	100W
21	Silicon Nitride	SiH_4	10	280°C	30min	300mTorr	75W
		NH_3	27.5				
22	”	”	”	”	”	400mTorr	”
23	”	”	”	”	”	500mTorr	”
24	”	”	”	”	”	600mTorr	”
25	”	”	”	”	”	700mTorr	”

3.2.2 Implementation

The first experiments were performed at 280°C using flow rates of 10 sccm of silane and 27.5 sccm of ammonia (for silicon nitride) or 30 sccm of nitrous oxide (for silicon dioxide). Power was kept constant at 75W and the tuning network was adjusted to minimize the reflected power. Pressure was varied by constricting the exhaust outlet of the chamber with the aforementioned valve. The pressures used for growth were 700mTorr, 600mTorr, 500mTorr, 400mTorr, and the baseline of the chamber which was approximately 300mTorr for each film type. Each film was grown for 30 minutes at each of these pressures.

Experiments were performed similar to the first except with pressure held constant and RF power varied. Pressure was held at 500mTorr, temperature remained the same, at 280°C and the same flow rates of silane and ammonia or nitrous oxide were used. The RF power was set to 20W, 40W, 60W, 80W, and 100W of forward power. The tuning network was adjusted until the reflected power was at a minimum (this ranged anywhere from 0 to 15W, depending on the desired forward power).

All experiments were performed as similarly as possible. The operating procedure used for every experiment is discussed in detail in Appendix A.

3.3 Results

3.3.1 Expectations

The effects of RF power and pressure on the growth rate of silicon dioxide and silicon nitride films was researched for comparison. Increasing deposition rate with pressure (12) and decreasing deposition rate with power density (2) were previously reported. Decreasing refractive index with power density (2) had also been reported. The refractive index of silicon nitride layers can vary greatly from growth to growth, but tends to stay in the 1.8-2.3 range (9). This variation has been shown to be affected by the silane flow rate in processes utilizing ammonia as a reactant and nitrogen gas a dilutant (7).

3.3.2 Comparison

The graphs of Figure 3.2 show the thicknesses measured for the pressure experiments. The thickness of these films were measured with a Nanospec Thin Film Measurement System (blue, center field), a KLA-Tencor Alpha Step 200 profilometer (green, right field), and a Perkin-Elmer Lambda 9 Spectrophotometer (orange, left field). The Lambda 9 thicknesses were calculated by adjusting the thickness and refractive index of the mathematical model for one layer of insulator on a substrate of crystalline silicon to best fit the measured Lambda 9 spectrum. The results from these best fit alignments are shown in Appendix B.

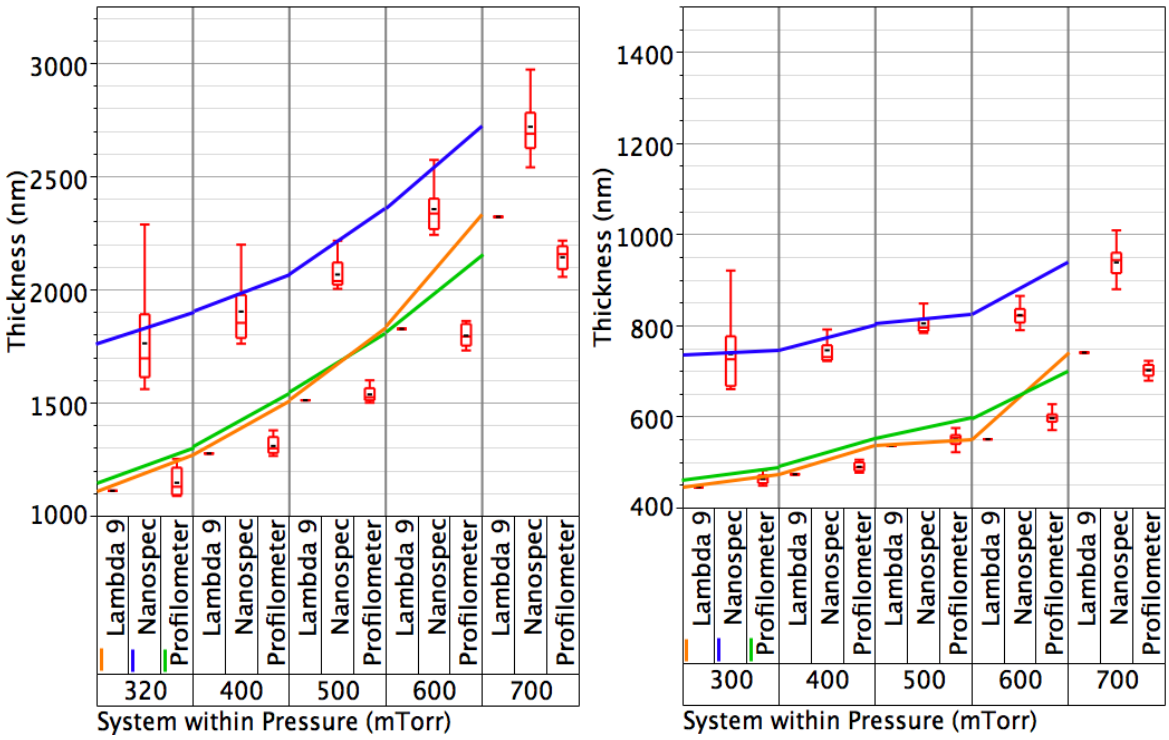

Figure 3.2 Silicon dioxide and silicon nitride by pressure

The results of the RF power experiments for silicon dioxide and silicon nitride are shown in Figure 3.3. The results show alignment with the research results noted previously. Growth rate increased with pressure and decreased with RF power.

These experiments were also analyzed for their refractive index based on the Lambda 9 measurements best fit analysis. The refractive indices of silicon dioxide (left graphs) films and silicon nitride films (right graphs) by pressure (top graphs) and RF power (bottom graphs) are shown in Figure 3.4. The results of this experiment are also in alignment with previous reports that refractive index would decrease with RF power and that the refractive index of silicon nitride can vary from run to run.

3.3.3 Conclusion

In order to balance the growth rate of silicon dioxide and silicon nitride the final growth parameters were determined as shown in Table 3.3. A pressure of 500mTorr was chosen as the

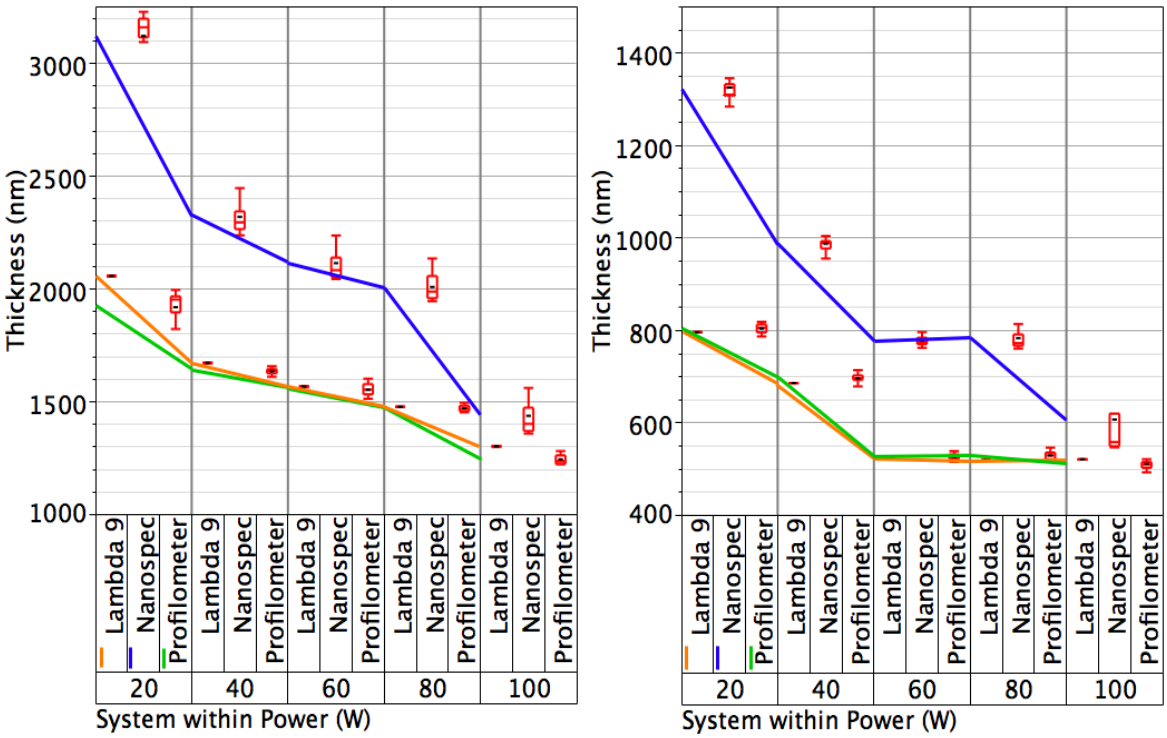

Figure 3.3 Silicon dioxide and silicon nitride by power

films grown at this level had the smallest standard deviation of thickness and the profilometer and Lambda 9 measurements aligned the closest at this point. The ability to stabilize the RF power above 80W became difficult and films grown between 60W and 80W had similar thicknesses measured by the Lambda 9 and profilometer. The inaccuracy of the Nanospec measurements is due to the fact that this system utilizes assumed refractive indices for the films it measures.

Table 3.3 Final growth parameters

Process	**Gas**	**Flow (sccm)**	**Chamber Pressure**	**Platen Temp**	**Power Level**
Silicon Nitride	SiH_4	10	500mTorr	280°C	75W
	NH_3	27.5			
Silicon Dioxide	SiH_4	10	500mTorr	280°C	75W
	N_2O	30			

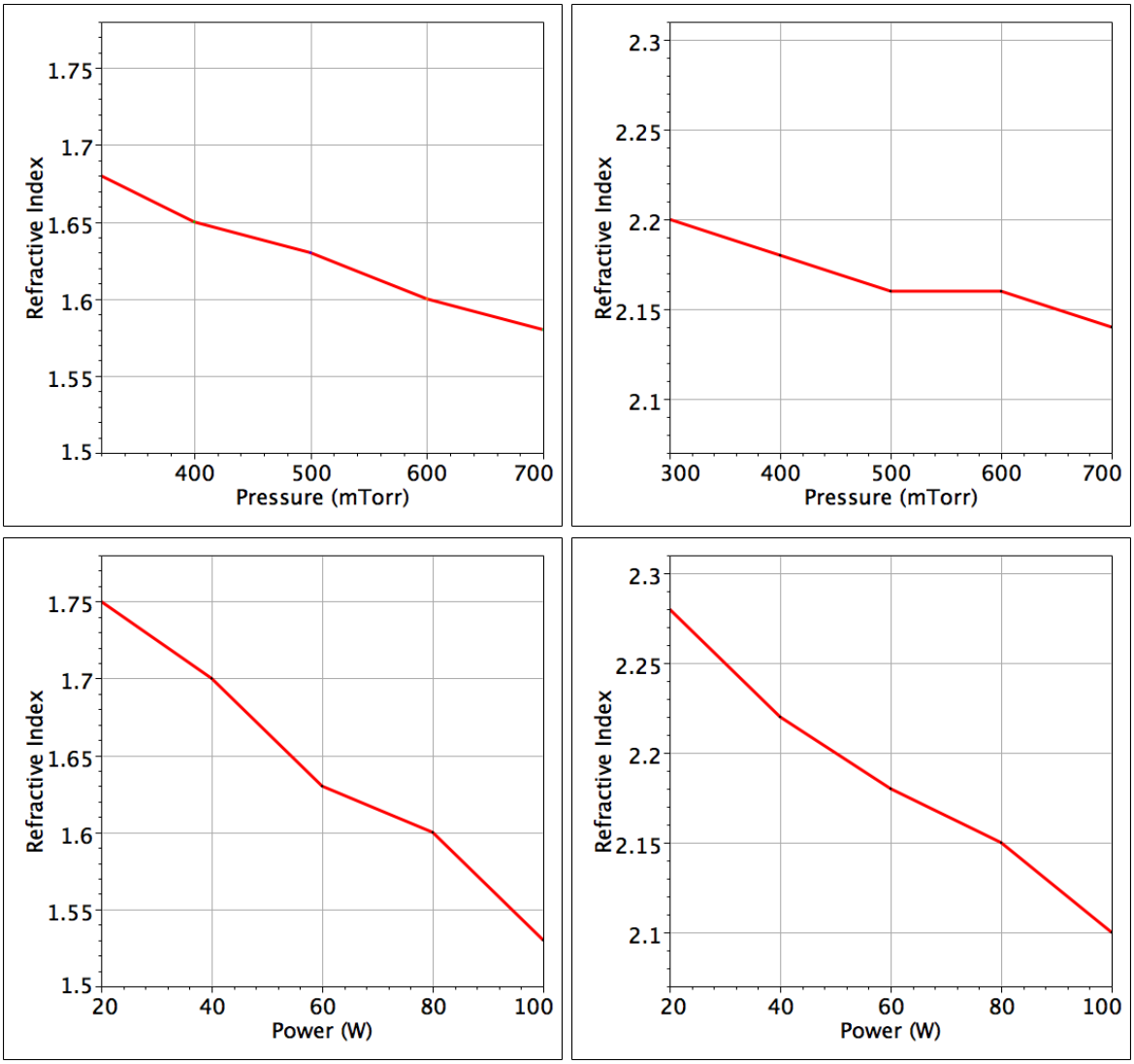

Figure 3.4 Silicon dioxide (left) and silicon nitride (right) refractive index by pressure (top) and by RF power (bottom)

CHAPTER 4. DBR

4.1 Theory

A recipe for the creation of DBRs was found through the results of PECVD experiments. Based on the 500mTorr measurements in the pressure variation experiment, the growth rates of silicon dioxide and silicon nitride were determined to be 50nm/min and 17.5nm/min respectively. With a calculated refractive index for silicon dioxide of 1.63 and 2.16 for silicon nitride, a DBR was designed for peak reflectance at a free-space wavelength of 580nm. A 5-layer pair DBR was designed with thicknesses of 89nm and 67nm for the silicon dioxide and silicon nitride layers, respectively. The recipe that was designed is shown in Table 4.1.

Table 4.1 DBR growth parameters

Process	**Gas**	**Flow (sccm)**	**Chamber Pressure**	**Platen Temp**	**Power Level**	**Time**
Silicon Nitride	SiH_4	10	500mTorr	280°C	75W	3min 50sec
	NH_3	27.5				
Silicon Dioxide	SiH_4	10	500mTorr	280°C	75W	1min 47sec
	N_2O	30				

4.2 Results

The first experiment performed with these conditions was broken up into the ten individual growths to allow measurement of each layer. One glass slide was placed inside the chamber along with one quarter-wafer of silicon. The glass slide remained in the chamber for all ten growths while a new quarter-wafer of silicon was placed inside the chamber for each growth. The results of thickness measurements on the ten silicon wafers is shown in Table 4.2. The

thicknesses were measured with the profilometer only, as they were too thin for the Nanospec and Lambda 9 to measure accurately.

Table 4.2 DBR growth results

Wafer	Film	Thickness	Wafer	Film	Thickness
1	Si_3N_4	68.7nm	2	SiO_2	79.3nm
3	Si_3N_4	63.4nm	4	SiO_2	86.4nm
5	Si_3N_4	67.7nm	6	SiO_2	87.0nm
7	Si_3N_4	72.4nm	8	SiO_2	85.8nm
9	Si_3N_4	67.6nm	10	SiO_2	88.7nm
AVG	**Si_3N_4**	**67.96nm**	**AVG**	**SiO_2**	**85.44nm**

The glass slide was measured for reflectance on the Lambda 9 spectrophotometer. The spectrum can be seen as Slide 1 in Figure 4.1. Two modeled spectra calculated from the computer program are also shown in this figure. The "Theoretical Model" spectrum is based on the designed thicknesses and measured refractive indices of the silicon dioxide and silicon nitride layers discussed earlier. The "Measured Thickness" spectrum is based on the measured thicknesses and refractive indices of the layers. Comparatively, the actual slide has a higher reflectance, but similar full width at half maximum as the measured thickness model. The measured thickness model proves to have a more similar shape to the actual spectrum than the theoretical model. The difference in reflectance proves the inaccuracy of the calculated refractive indices used to model this DBR, as the peak reflectance does not change between the two models, which used the same refractive indices, but different thicknesses.

A second and third DBR were grown in a second experiment using an unopened chamber. Unlike the first experiment there were no silicon wafers added to measure the thickness of each layer. The experiment utilized the same recipe as shown in Table 4.1. The spectra of the DBR from the first experiment (Slide 1) and the two DBRs from the second experiment (Slides 2 and 3) are shown in Figure 4.2.

A comparison of Figures 4.1 and 4.2 lends itself to the conclusion that the refractive indices of the two PECVD grown materials varies from run to run and even within a run. This is evidenced by the different peak reflectances of the three slides. A simple formula for the peak

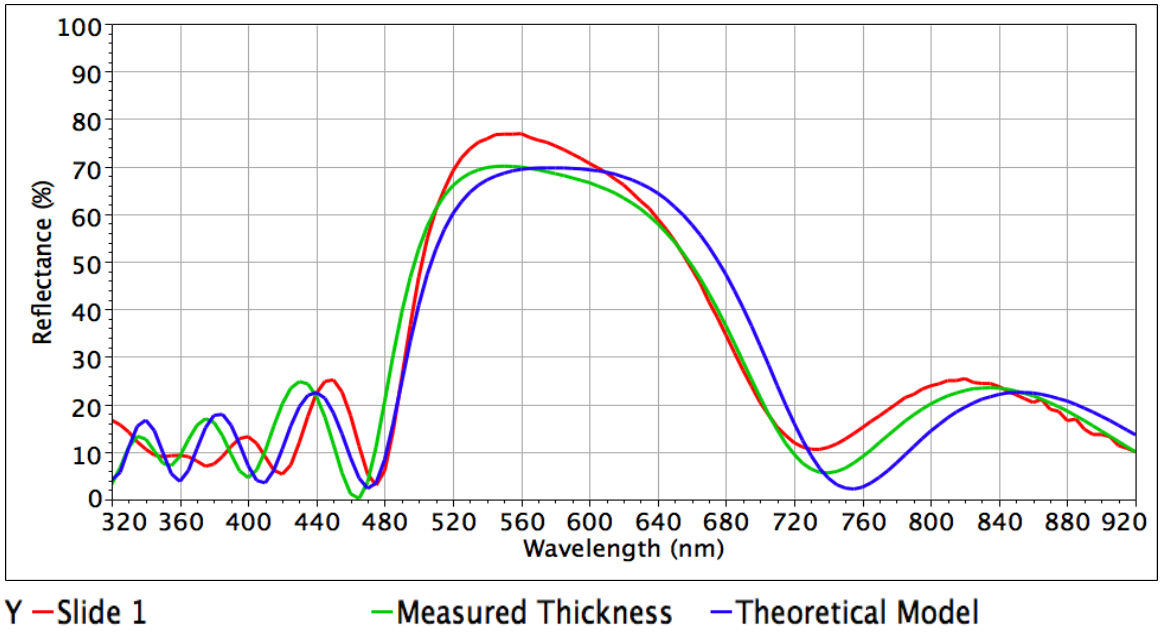

Figure 4.1 Five layer pair DBR spectra

reflectance of a DBR is shown in Equation 4.1 which is related only to the refractive indices of the two materials (n_1 and n_2) and the surrounding medium (n_0) and substrate (n_s), in this instance, silicon dioxide, silicon nitride, air, and glass, respectively.

$$R = \left[\frac{n_0 \left(n_2\right)^{2N} - n_s \left(n_1\right)^{2N}}{n_0 \left(n_2\right)^{2N} + n_s \left(n_1\right)^{2N}}\right]^2 \tag{4.1}$$

Despite the differences between these three DBRs created with the same procedure, they will make excellent reflectors for a microcavity. Additionally, the relatively wide bandwidth of the spectra allow for the same reflectors to be used for microcavities with different modal frequencies. The overall thickness of the microcavity, not the reflector alone, will narrow the frequency down to the specific value desired. This flexibility could allow for the creation of several microcavity OLED pixels on one substrate, each with a different modal frequency.

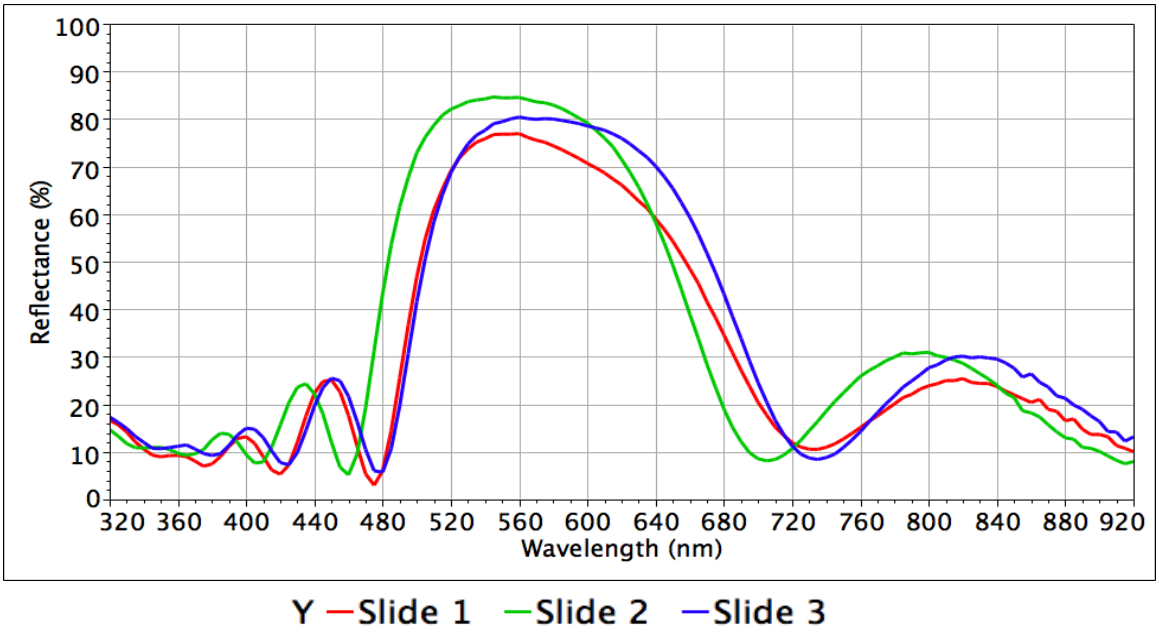

Figure 4.2 Five layer pair DBR spectra from three slides

CHAPTER 5. SUMMARY AND DISCUSSION

5.1 Conclusion

The method for creation of distributed Bragg reflectors in this project proved to be quite a flexible process. Experiments were performed to determine the optimum growth parameters for the PECVD system to be used. Parameters were chosen to reduce variations between runs, but the system is imperfect. Despite the variations in film thickness and refractive index, the reflectors had very similar spectra and all would be of excellent quality as reflectors in microcavities. Determining the refractive indices of the silicon dioxide and nitride films, however, was a more difficult task. Without access to a modern ellipsometer, these measurements were performed through the mathematical analysis of spectrophotometer readings as shown in Appendix B. The work was subjective, leading to indeterminate inaccuracies in the DBR calculations. Despite these shortcomings the DBRs performed perfectly and their specifications appear to be reproducible to within 10%. The three slides had reflectance of between 75% and 85% with full widths at half maximum of 170-180nm centered around 570-590nm when they were designed to be centered at 580nm. The reflectors could be made in batches of up to 4 glass slides at a time, with a total process time of less than one hour.

5.2 Future Work

The creation of more DBRs using this method should prove a viable base for the creation of microcavity OLED photoluminescent sensors. A method for the deposition of indium tin oxide onto the DBR substrates is available at the Microelectronics Research Center. In order to incorporate the indium tin oxide into the microcavity, this method needs to be characterized for its optical properties and growth rate, for the deposition of accurate thicknesses of the

material. Once this is achieved, the OLED can be manufactured on top of the DBR by Joseph Shinar's research group. The thickness of the OLED does not necessarily need to be extremely accurate, as more silicon nitride could be deposited on top of it as a filler to achieve the proper microcavity thickness. However, the refractive index of the OLED material needs to be measured so that the microcavity can be designed accordingly. Finally the aluminum cathode/reflector needs to be deposited and the OLED microcavity would be complete and ready for analysis.

The PECVD system used in this project could become a valuable asset to the Microelectronics Research Center if the silicon dioxide and silicon nitride films it produces were characterized more completely. For this project only the optical properties of the materials were important, but other uses of these films may require better electrical or physical properties. The resistance, permittivity, and hardness of these films could be measured and characterized. Other adjustments to the growth parameters could be made, such as the inclusion of helium into the silicon dioxide growth as this has shown to reduce the growth rate and allow for films with electrical properties much closer to those of thermally grown silicon dioxide (1).

APPENDIX A. PECVD STANDARD OPERATING PROCEDURES

A.1 System Preparation

The Technics 900 Series Plasma Enhanced Chemical Vapor Deposition System is shown in Figure A.1. The white box behind the PECVD machine is the gas control chamber. The exhaust hose behind the PECVD system leading down and out of the picture is connected to a mechanical vacuum pump.

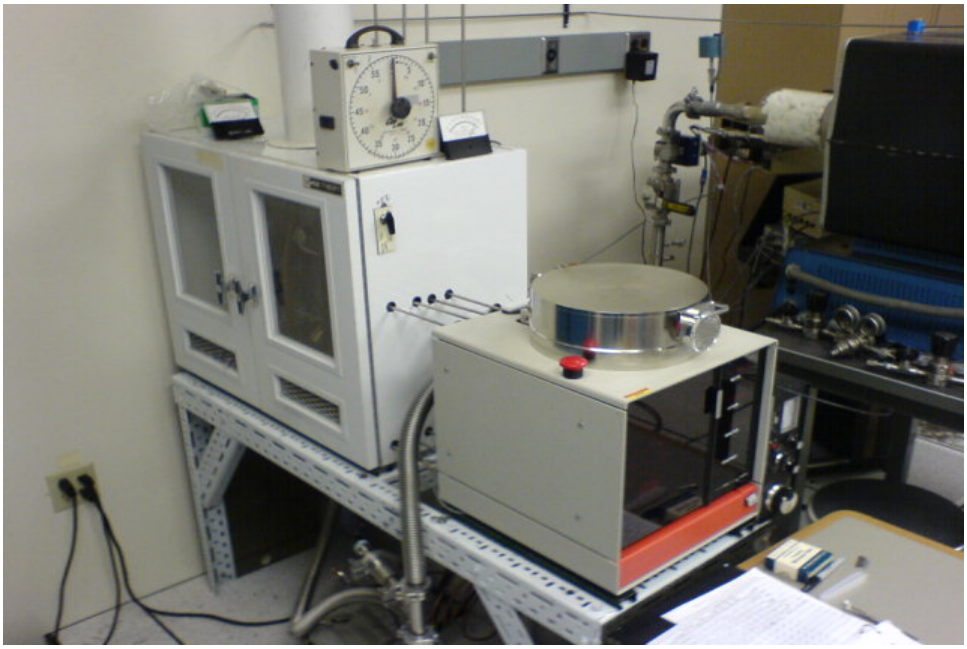

Figure A.1 PECVD system

Inside the gas control chamber are valves to control the supply of process gases (SiH_4, NH_3, N_2O) and the vent gas (N_2). Because silane is used in this system and silane is pyrophoric, nitrogen is used as the pressurized gas for all pneumatic valves contained in the system, rather

than air, so that if a valve were to fail, it would not combust.

Before running the system some preparations must be made. Outside of the cleanroom the nitrogen dewar must be opened. Nitrogen is not reactive with silane, so is used as the dilutant in gas processes requiring the use of silane. Inside the gas control chamber the vacuum pump purge valve and vent valve must be opened. The valves to the gases required for deposition should also be valved open at this time. The inside of the gas control chamber is shown in Figure A.2.

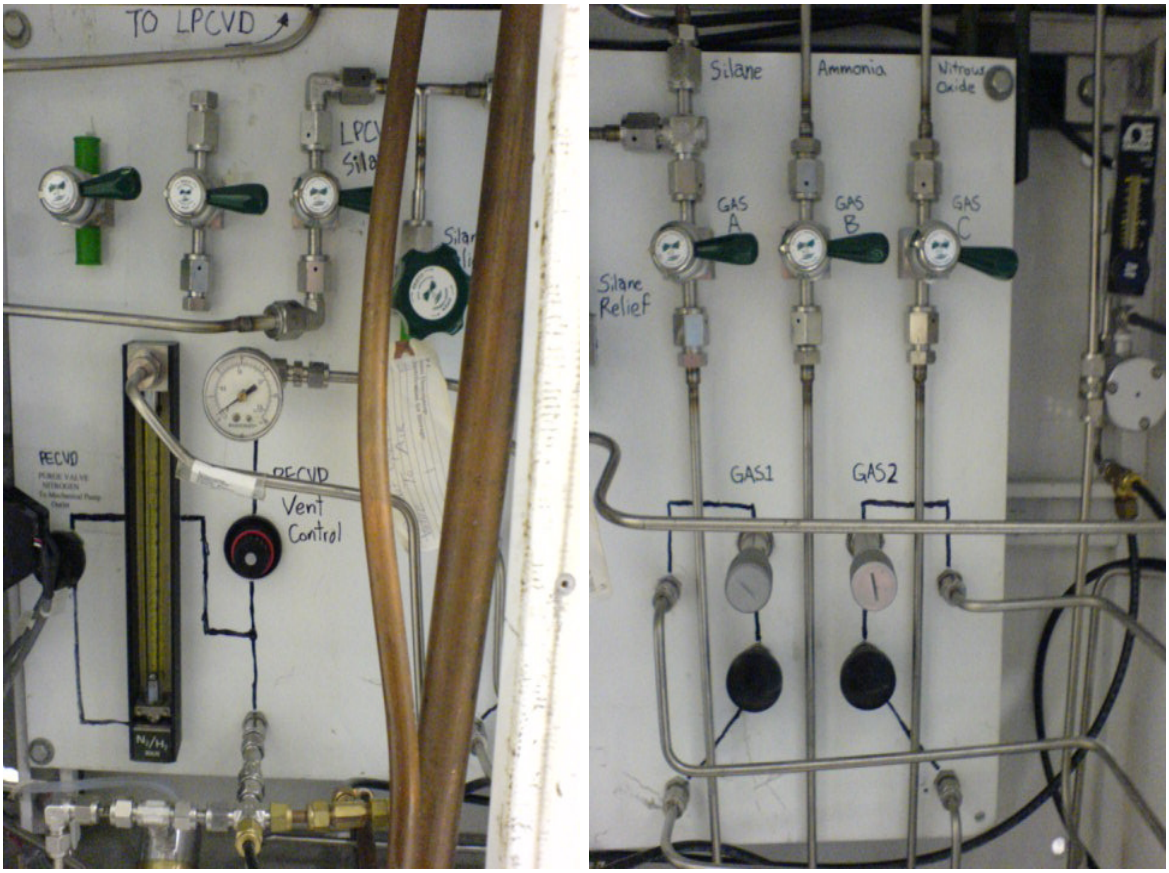

Figure A.2 Gas control cabinet

Outside the gas control chamber, the silane control valve must be turned on, this stops the flow of silane if there is a sudden loss of nitrogen pressure. The mechanical pump may now be turned on and the purge valve on the mechanical pump opened. Next, the vacuum valve on the back of the PECVD system can be opened fully and the PECVD system started by

pressing the power button located on the back right side of the system.

In preparation for a run, the temperature controller should be set and turned on. The vacuum valve should be opened to allow the chamber to be pumped down. Allow the chamber to pump down to approximately 40mTorr and the temperature controller to reach the desired set point before continuing, this should take less than 30 minutes.

A.2 Chamber Loading/Unloading

Before loading or unloading the chamber, it is important to purge any silane that may still be present so as to avoid combustion with air. With the vacuum valve open, open the vent valve 2-3 times for approximately five seconds at a time. This will fill the chamber with nitrogen. Allow the vacuum pump to bring the pressure back down to below 100mTorr before opening the vent valve each time. It is suggested that the chamber be purged both before and after the chamber is opened, to remove silane from the chamber when opening and to remove air from the chamber when closing.

Figure A.3 PECVD controls

A.3 Operation

The pressure and flow rates can change from run to run and set points can move, especially when the system has been sitting, powered down, for some time. It is important, therefore, to perform a parameter setting run. Before running the system with the substrates in the chamber, a run should be performed with an empty chamber to adjust the levels of flows and the pressure level. Two minutes of running the system should be adequate to get the parameters correct. The front controls of the system are shown in Figure A.3. The controls behind the tinted door are for gas flow and temperature. The controls behind the orange panel are for the chamber. While the flow controls set the flow rates, the chamber controls actually valve the gases into the chamber.

Figure A.4 PECVD flow rate controls

To start a run, make sure the system is pumped down to approximately 40mTorr and the temperature has reached its set point. The flow control section is shown in Figure A.4. Adjust the flow rates to the desired value by turning the switch to the left of the flow gauge to "SET" and turn the switch to the right of the gauge to the gas to be set and adjust the "CAL" dial

for that gas. Do this for each gas to be used. Turn the switch to the left of the gauge to read, and flip the "AFC/GAS 1" switch to "GAS 1" and turn on the switches for the gases required.

Figure A.5 shows the controls behind the orange panel. Now that the flows are set they can be diverted into the chamber, by turning the "GAS #1" (located behind the orange panel) switch to on. Gas is now flowing into the chamber. Once the pressure stabilizes, the pressure can be adjusted to the desired level. The rotary valve on the back of the chamber can be tightened until the pressure reaches the desired point. Next the RF power can be started. The "LEVEL" knob should be turned completely counterclockwise, then the "POWER" switch turned on. Slowly turn the "LEVEL" knob clockwise to increase the power.

Figure A.5 PECVD chamber controls

The controls of the tuning network are shown in Figure A.6. Once the power reaches the desired level, adjust the roller inductor, transmitter, and antenna knobs on the tuning network to minimize the reflected power, once this is achieved readjust the power to the desired set point on the PECVD system. At this point the plasma glow should be visible through the small circular window of the chamber.

Now that the power is set and a plasma is achieved, the pressure has most certainly changed, adjust, again, the rotary valve on the back of the chamber to the desired pressure level. Now the system is set to the parameters required for film growth. Turn off the "POWER" switch and "GAS #1" switch, respectively. Next the chamber can be opened and loaded with substrates per the directions in the previous section.

Figure A.6 PECVD tuning network controls

When running the system for deposition, since all the parameters are set, simply wait for the temperature to stabilize to the set point and the pressure to below 40mTorr. Next, open the "GAS #1" switch and allow the pressure to stabilize. Finally, switch on the "POWER" and start a timer for the desired time for deposition. Once the time has expired, turn off the "POWER" and "GAS #1" valves in that order.

A.4 Shutdown

When the system is finished being used, it must be shutdown properly. Turn off all gas flows in the flow control area on the front of the PECVD system, set the "AFC/GAS 1" switch to AFC. Make sure the gas valve controls behind the orange panel are closed. Close the "VAC" valve in the valve control area and close the rotary valve at the back of the chamber. The PECVD system can now be shutdown by pressing the red emergency shut off switch located next to the chamber on top of the system. The gas valves in the gas control cabinet can now be closed. The nitrogen purge valve on the mechanical pump should be closed and the mechanical pump shut off before the purge valves in the gas control chamber are closed. Finally, the silane control valve can be closed and the nitrogen dewar located outside of the cleanroom closed.

A.5 Growth Parameters

Table A.1 PECVD growth parameters

Process	**Gas**	**Flow (sccm)**	**Chamber Pressure**	**Platen Temp**	**Power Level**	**Growth Rate**
Silicon Nitride	SiH_4	10	500mTorr	280°C	75W	17.5nm/min
	NH_3	27.5				
Silicon Dioxide	SiH_4	10	500mTorr	280°C	75W	50nm/min
	N_2O	30				

APPENDIX B. PECVD EXPERIMENT RESULTS: REFRACTIVE INDEX MEASUREMENT

Shown here are the reflectance spectra for each of the 20 experimental layers grown and the modeled reflectance (in red) adjusted to best fit the Lambda 9 data (in blue). The refractive index and layer thickness required to achieve this alignment is noted below each spectrum.

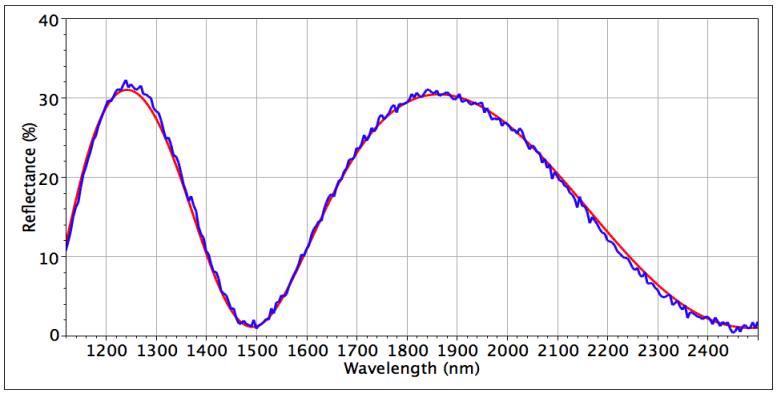

Figure B.1 Wafer 1 SiO_2 - Thickness: 1110nm, Refractive Index: 1.68

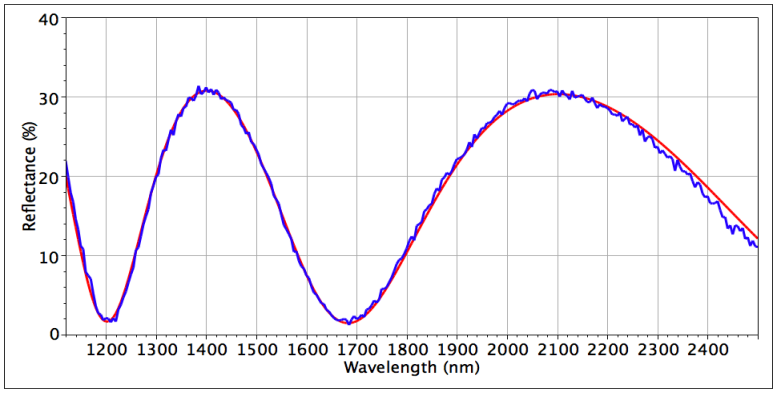

Figure B.2 Wafer 2 SiO_2 - Thickness: 1275nm, Refractive Index: 1.65

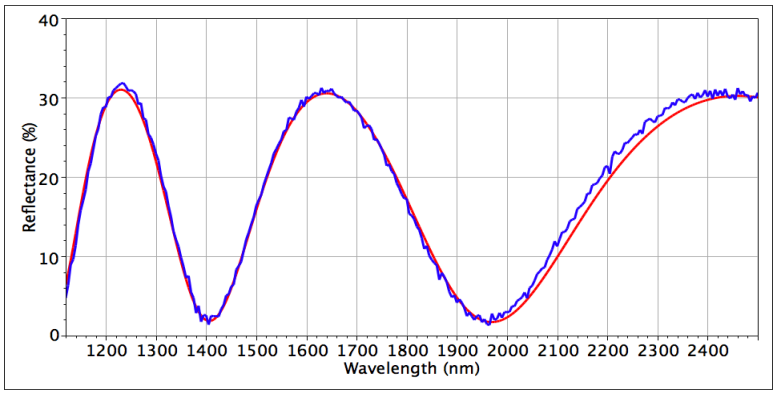

Figure B.3 Wafer 3 SiO_2 - Thickness: 1510nm, Refractive Index: 1.63

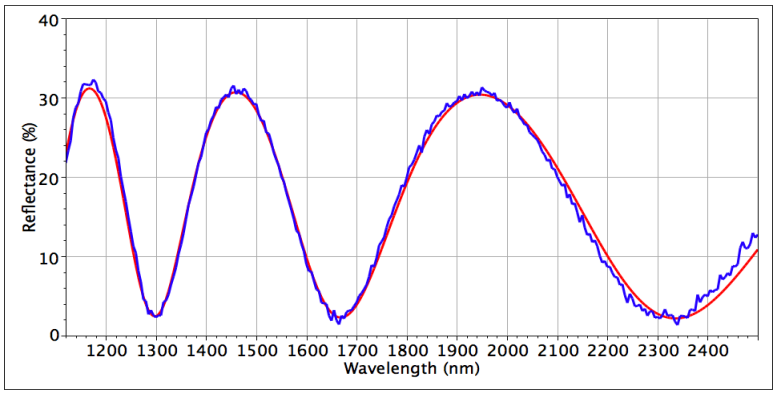

Figure B.4 Wafer 4 SiO_2 - Thickness: 1825nm, Refractive Index: 1.60

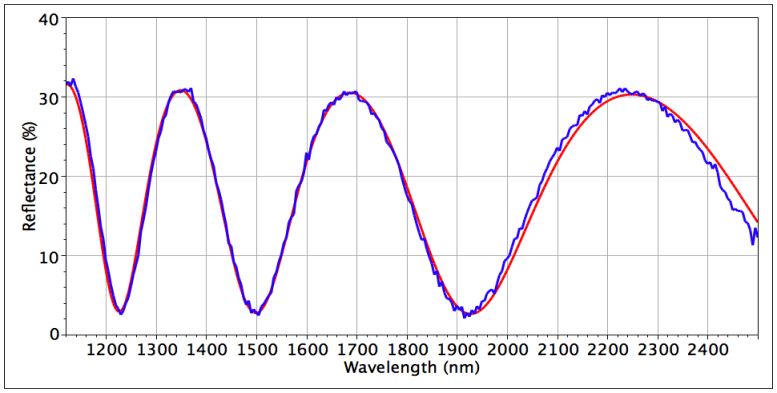

Figure B.5 Wafer 5 SiO_2 - Thickness: 2135nm, Refractive Index: 1.58

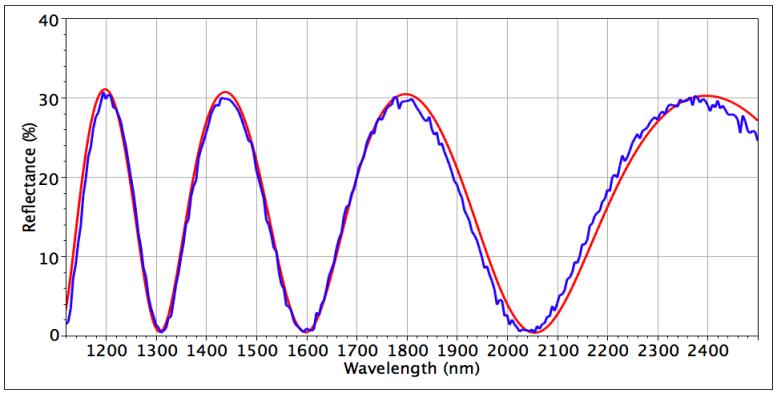

Figure B.6 Wafer 6 SiO_2 - Thickness: 2055nm, Refractive Index: 1.75

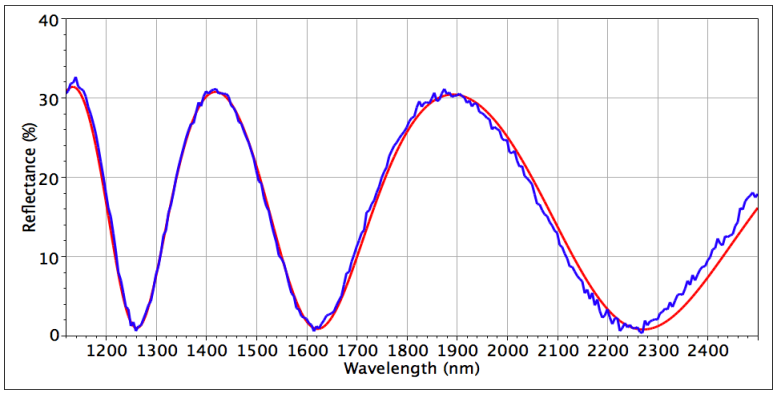

Figure B.7 Wafer 7 SiO_2 - Thickness: 1670nm, Refractive Index: 1.70

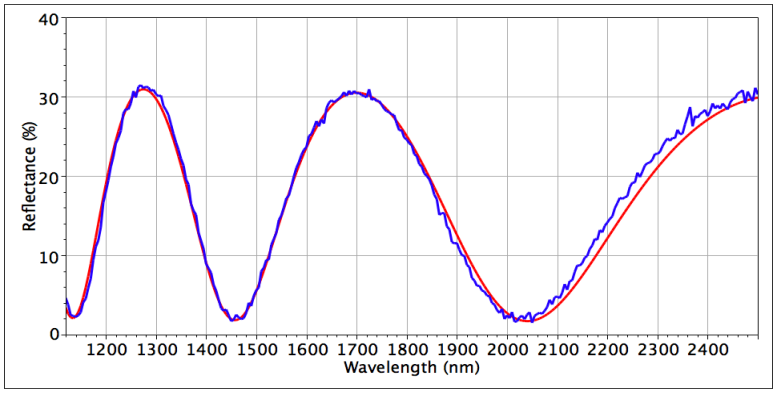

Figure B.8 Wafer 8 SiO_2 - Thickness: 1565nm, Refractive Index: 1.63

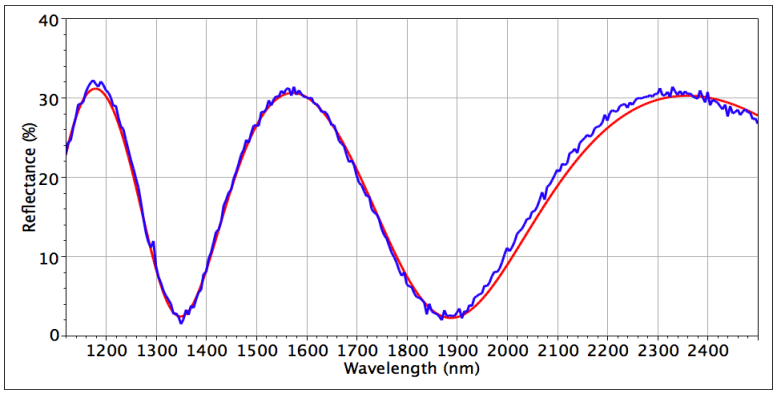

Figure B.9 Wafer 9 SiO_2 - Thickness: 1475nm, Refractive Index: 1.60

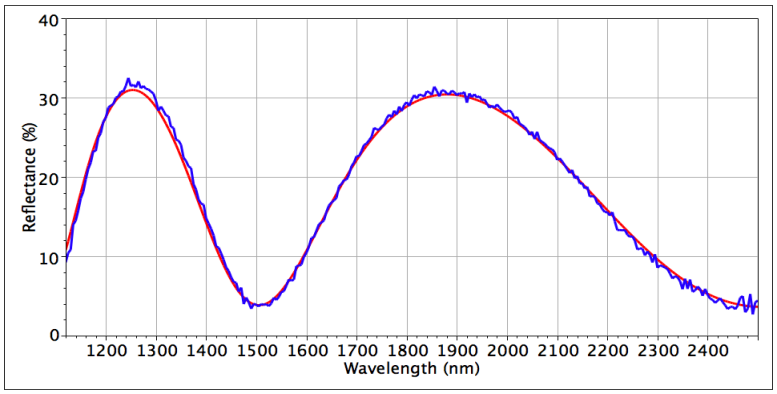

Figure B.10 Wafer 10 SiO_2 - Thickness: 1230nm, Refractive Index: 1.53

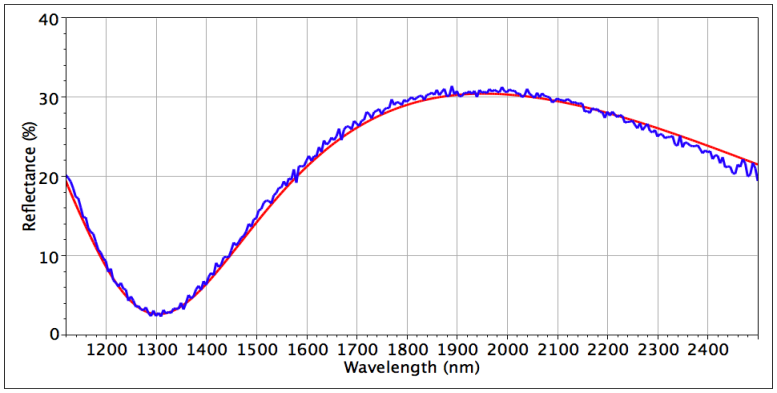

Figure B.11 Wafer 16 Si_3N_4 - Thickness: 445nm, Refractive Index: 2.20

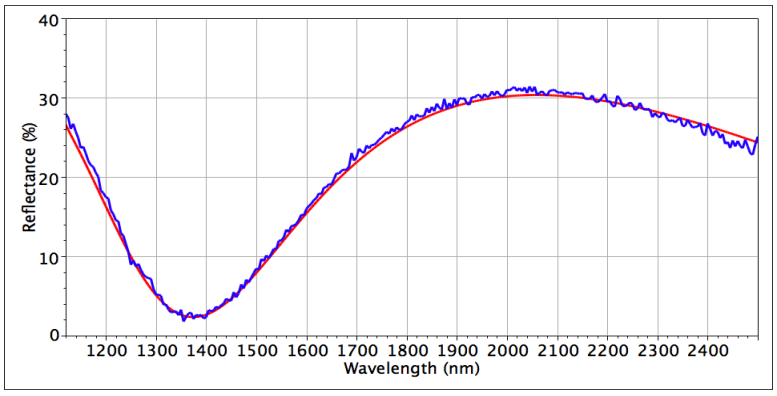

Figure B.12 Wafer 17 Si_3N_4 - Thickness: 473nm, Refractive Index: 2.18

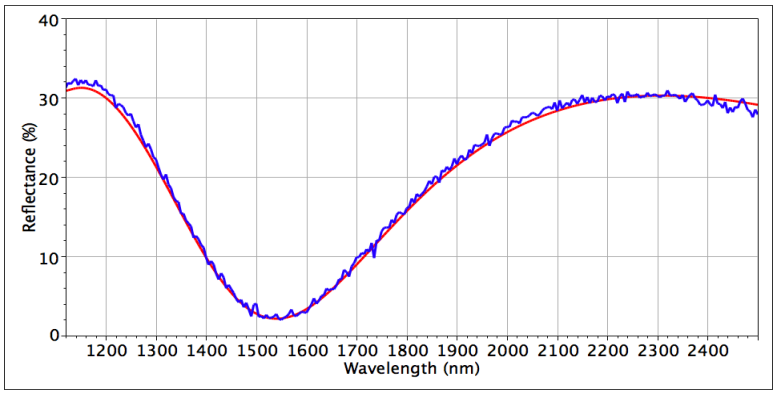

Figure B.13 Wafer 18 Si_3N_4 - Thickness: 535nm, Refractive Index: 2.16

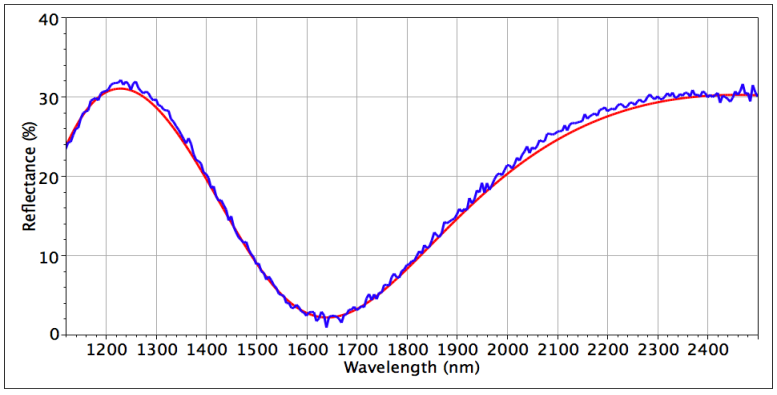

Figure B.14 Wafer 19 Si_3N_4 - Thickness: 550nm, Refractive Index: 2.16

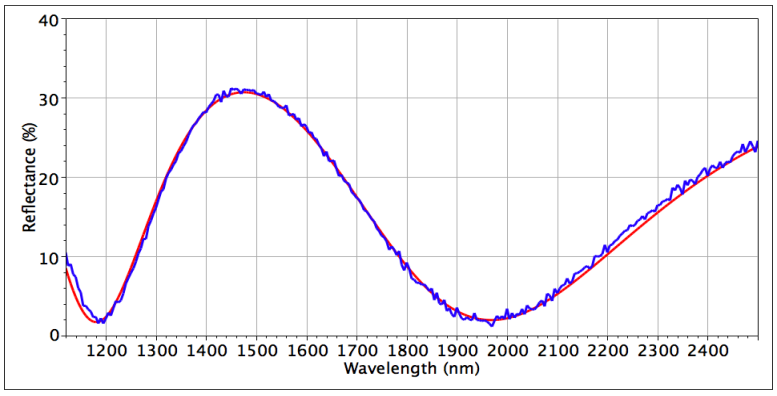

Figure B.15 Wafer 20 Si_3N_4 - Thickness: 690nm, Refractive Index: 2.14

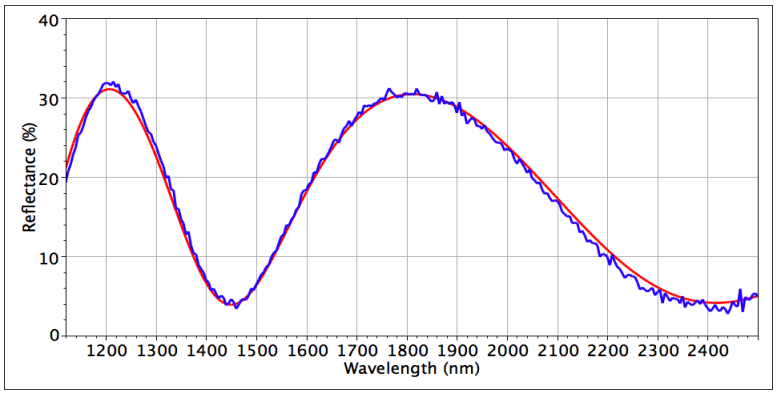

Figure B.16 Wafer 21 Si_3N_4 - Thickness: 795nm, Refractive Index: 2.28

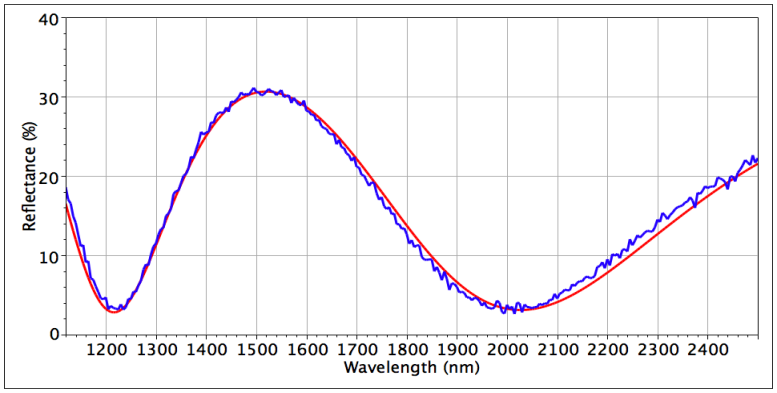

Figure B.17 Wafer 22 Si_3N_4 - Thickness: 685nm, Refractive Index: 2.22

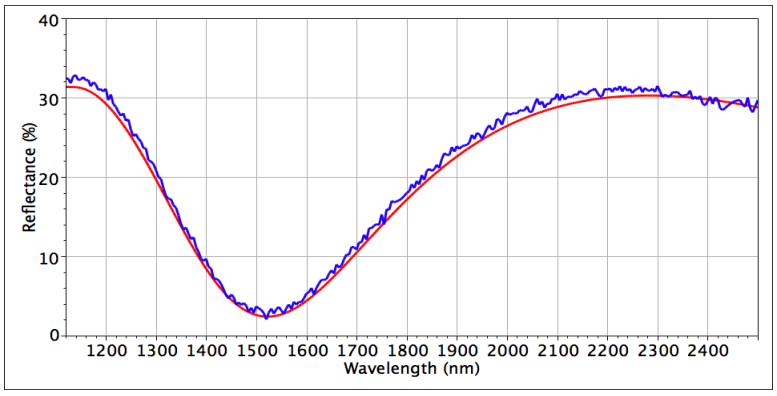

Figure B.18 Wafer 23 Si_3N_4 - Thickness: 524nm, Refractive Index: 2.18

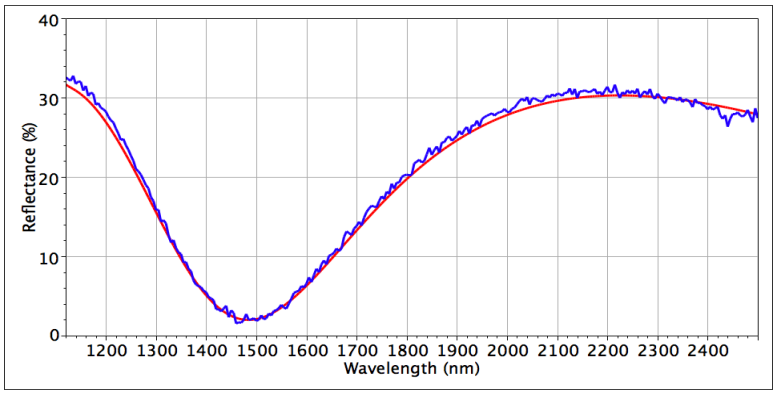

Figure B.19 Wafer 24 Si_3N_4 - Thickness: 518nm, Refractive Index: 2.15

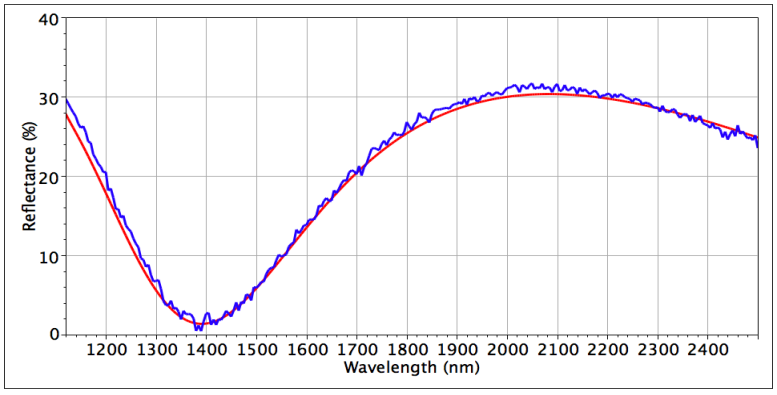

Figure B.20 Wafer 25 Si_3N_4 - Thickness: 497nm, Refractive Index: 2.10

BIBLIOGRAPHY

[1] Batey, J. and E. Tierney (1986). "Low-temperature deposition of high-quality silicon dioxide by plasma-enhanced chemical vapor deposition." *Journal of Applied Physics 60*(9): 3136-3145

[2] Chapple-Sokol, J. D. , E. Tierney, and J. Batey (1990). "RF Power Dependence of the Material Properties of PECVD Silicon Dioxide." *Materials Research Society Symposium Proceedings*, *165*, 113–118.

[3] Cheng, David K. (1989). *Field and Wave Electromagnetics* Reading, MA: Addison-Wesley Publishing Company, Inc.

[4] Choudhury, Bhaskar, Ruth Shinar, Joseph Shinar (2004). "Glucose biosensors based on organic light-emitting devices structurally integrated with a luminescent sensing element." *Journal of Applied Physics 96*(5), 2949–2954.

[5] Dodabalapur, Ananth (2004). *Organic Light-Emitting Devices: A Survey* New York, NY: Springer.

[6] Kasap, Safa O. (2001). *Optoelectronic Devices and Photonics: Principles and Practices.* Upper Saddle River, NJ: Prentice-Hall, Inc.

[7] Konuma, Mitsuharu (2005). *Plasma Techniques for Film Deposition.* Harrow, UK: Alpha Science International Ltd.

[8] Lai, Q. , J. S. Gu, M. K. Smit, J. Schmid and H. Melchior (1992). "Simple technologies for fabrication of low-loss silica waveguides." *IEEE: Electronics Letters 28*(11): 1000-10001.

[9] Pliskin, W. A. (1987). "Refractive index dispersion of dielectric films used in the semiconductor industry." *Journal of the Electrochemical Society. 134* (11): 2819-2826.

[10] Smith, Donald L (1993). "Controlling the plasma chemistry of silicon nitride and oxide deposition from silane." *Journal of Vacuum Science and Technology A 11* (4): 1843-1850

[11] *Technics Micro-Plasma Deposition Series 900 Plasma System: Instruction Manual* (1989) Technics Inc. Dublin, CA.

[12] Varhue, W. J. and K. A. Pandelisev (1990). "The Effect of Reactor Pressure on the Growth of Glow Discharge a-SiN:H." *Materials Research Society Symposium Proceedings*, *165*, 29–34.